MNRAS 000, 1–13 (2022) Preprint 11 April 2022 Compiled using MNRAS LATEX style file v3.0

Binarity Enhances the Occurrence Rate of Quiescent Radio Emission in Ultracool Dwarfs

Melodie Kao,[1,2,3,4]★ J. Sebastian Pineda[5]
[1]*Arizona State University, School of Earth and Space Exploration, 550 E Tyler Mall PSF 686, Tempe, AZ 85287*
[2]*University of California Santa Cruz, Department of Astronomy amd Astrophysics, 1156 High Street, Santa Cruz, CA 95064*
[3]*NASA Hubble Postdoctoral Fellow*
[4]*Heising-Simons 51 Pegasi b Fellow*
[5]*University of Colorado Boulder, Laboratory for Atmospheric and Space Physics, 3665 Discovery Drive, Boulder CO, 80303, USA*

Accepted XXX. Received YYY; in original form ZZZ

ABSTRACT

The initial discovery of strong radio activity from ultracool dwarfs with spectral type >M7 was a surprise that led to a new auroral paradigm in our understanding of magnetic activity in the mass range that bridges planets and stars. Despite a burgeoning set of ultracool dwarf radio detections, their radio emissions remain enigmatic. Open questions include the source and acceleration mechanisms for the non-auroral "quiescent" component of these objects' radio emissions. Ultracool dwarf binary systems can provide test beds for examining the underlying physics for these plasma processes. We extend a recently developed occurrence rate calculation framework to compare the quiescent radio occurrence rate of binary systems to single objects. We combine data available in the literature to create samples of 179 single ultracool dwarfs (82 M dwarfs, 75 L dwarfs, and 23 T/Y dwarfs) and 28 binary ultracool dwarf systems. Using these samples, we show that binarity enhances the ultracool dwarf quiescent radio occurrence rate relative to their single counterparts. Finally, we discuss potential implications for the underlying drivers of ultracool dwarf quiescent radio emissions, including possible plasma sources.

Key words: brown dwarfs — planets and satellites: magnetic fields — radio continuum: stars — stars: magnetic fields

1 INTRODUCTION

Magnetic activity undergoes a fundamental shift as ultracool dwarfs (>M7) drop in effective temperature and become more planet-like. Ultracool dwarfs at late as ~T6.5 (Route & Wolszczan 2012; Kao et al. 2016; Williams et al. 2017; Vedantham et al. 2020) can produce bursting radio emission that is orders of magnitude stronger than predicted by coronal X-ray emission (e.g. Berger et al. 2001; Williams et al. 2014; Pineda et al. 2017). A trio of papers recently argued that coherent and periodically bursting ultracool dwarf radio emission, emitted via the electron cyclotron maser instability (Hallinan et al. 2007, 2008), trace the radio component of aurorae in these objects (Hallinan et al. 2015; Kao et al. 2016; Pineda et al. 2017). Searches for such coherent emission from ultracool dwarfs have yielded the first direct discovery of a brown dwarf using radio observations (Vedantham et al. 2020), confirmed that late T dwarfs can host kiloGauss magnetic fields (Route & Wolszczan 2012, 2016a; Williams & Berger 2015; Kao et al. 2016, 2018; Richey-Yowell et al. 2020), and demonstrated that our understanding of dynamos in the mass and temperature regime bridging low mass stars and planets remains limited (Kao et al. 2016, 2018).

Ultracool dwarfs can also produce long-lived incoherent quasi-steady nonthermal radio emission (e.g., Williams et al. 2015a; Kao et al. 2016, 2018), which numerous studies attribute to optically thin gyrosynchrotron emission (e.g. Berger et al. 2005; Osten et al. 2006; Williams et al. 2015b; Lynch et al. 2016). Williams et al. (2015b) propose that blanket of low-level flaring may be one possible explanation for the quiescent component of ultracool dwarf radio emission, which extends to at least 95 GHz (Williams et al. 2015b; Hughes et al. 2021). Observations demonstrate that strong white-light flares can occur on early L dwarfs (e.g. Gizis et al. 2013; Paudel et al. 2018a; Jackman et al. 2019; Paudel et al. 2020). However, the possibility of such behavior extending to cooler objects remains unknown, as is also the case regarding the existence and rate of weaker radio flares in ultracool dwarfs.

Hallinan et al. (2006) postulated an alternative interpretation in which these objects' quiescent radio emission trace dense regions of energetic particles trapped in their large-scale magnetospheres, similar to the radiation belts possessed by magnetized solar system planets (Sault et al. 1997; Bolton et al. 2004; Clarke et al. 2004; Horne et al. 2008). In later work, Pineda et al. (2017) and Kao et al. (2019) develop this idea into a coherent framework tying together the auroral and quiescent components of ultracool dwarf radio emissions. One exciting implication of this framework is that satellite volcanism could be one possible source of plasma for ultracool dwarf radiation belts. Indeed, volcanic activity from

★ E-mail: melodie.kao@ucsc.edu

the moon Io is a major plasma source for the Jovian radiation belts (e.g. Horne et al. 2008), and theory predicts satellites around brown dwarfs (e.g. He et al. 2017; Sestovic & Demory 2020).

Recently, Kao & Shkolnik (submitted) argued for quantifying ultracool dwarf magnetic activity using their quiescent rather than periodically bursting auroral radio emission. They noted that the rarity of detected ultracool dwarf radio emission together with the wealth of data available in the literature underscored the value of moving toward studies of radio occurrence rates as a function of object characteristics, such as $T_{\rm eff}$, mass, rotation rate, and age. Volume-limited radio surveys yield detection rates between ~5–10% for M, L, and T ultracool dwarfs (Antonova et al. 2013; Lynch et al. 2016; Route & Wolszczan 2016b), though these studies do not separately treat binaries.

Kao & Shkolnik (submitted) developed an analytical framework for calculating occurrence rates for quiescent radio emission. By applying this framework to observations available in the literature, they show that ultracool dwarf quiescent radio occurrence rates are between $15^{+4}_{-4}\%$ – $20^{+6}_{-5}\%$ for isolated ultracool dwarfs. Furthermore, L dwarfs may have a suppressed radio occurrence rate compared to M and T/Y dwarfs.

To date, no comprehensive study of ultracool dwarf radio emission has focused on binaries, yet comparing the population of single objects to ultracool dwarf binaries provides a complementary means of identifying characteristics that influence magnetic activity at the stellar-planetary boundary. For instance, in stars, tidal spin-up may enhance the rotation rates and thus the magnetic activity of the binary population (Zahn 1977; Morgan et al. 2016). Here, we assess whether binarity enhances the quiescent radio occurrence rate of ultracool dwarfs in binary systems compared to their single counterparts.

2 EXTENDING AN OCCURRENCE RATE FRAMEWORK FOR SINGLE OBJECTS TO BINARY SYSTEMS

Does binarity affect the magnetic activity of ultracool dwarfs? To answer this question, we compare the quiescent radio occurrence rates for ultracool dwarfs in single-object versus binary systems by adapting the occurrence rate framework developed by Kao & Shkolnik (submitted). We use their notation here, where $\mathbb{P}$ denotes probability and $\mathcal{P}$ refers to a probability density distribution function.

This Bayesian occurrence rate framework for single objects considers the probability $\theta_{\rm single}$ that an object is emitting between an assumed luminosity range $L_\nu \in [L_{\rm min}, L_{\rm max}]$ for a dataset D consisting of individual observations where the $i^{\rm th}$ observation $D_i = \{\text{detect}_i, \sigma_{\text{rms}_\text{i}}, d_i, \sigma_{\text{d}_\text{i}}, L_{\nu,i}\}$. They treat each observation property as a random variable, where $\text{detect}_i \in \{0 \text{ if undetected}, 1 \text{ if detected}\}$, $\sigma_{\text{rms}_\text{i}}$ is the reported rms noise for each object, d_i is the distance to each object, $\sigma_{\text{d}_\text{i}}$ is the error for the measured d_i, and $L_{\nu,i}$ is the assumed specific luminosity for quiescent radio emission. They show that for single-object systems, the probability $\mathbb{P}(D \mid \theta_{\rm single})$ of observing a dataset given a fixed occurrence rate $\theta_{\rm single} = \Theta$ depends on the probability of drawing the particular observational and object properties captured in D:

$$\mathbb{P}(D \mid \theta_{\rm single} = \Theta) = \prod_{i=1}^{N} \mathbb{P}(\sigma_{\text{rms}_\text{i}})\, \mathbb{P}(\sigma_{\text{d}_\text{i}})\, \mathbb{P}(d_i) \times \begin{cases} \Theta\, \mathbb{P}(L_{\nu,i} \geq L_{\text{thr,i}} \mid \sigma_{\text{rms}_\text{i}}, \sigma_{\text{d}_\text{i}}, d_i, e = 1) & , \ \text{detect}_i = 1 \\ 1 - \Theta\, \mathbb{P}(L_{\nu,i} \geq L_{\text{thr,i}} \mid \sigma_{\text{rms}_\text{i}}, \sigma_{\text{d}_\text{i}}, d_i, e = 1) & , \ \text{detect}_i = 0 \end{cases} , \tag{1}$$

where $\mathbb{P}(L_{\nu,i} \geq L_{\text{thr,i}} \mid \sigma_{\text{rms}_\text{i}}, \sigma_{\text{d}_\text{i}}, d_i, e = 1)$ is the probability that the object has a detectable luminosity $L_{\text{thr,i}}$, and $e \in \{0 = \text{not emitting}, 1 = \text{emitting}\}$ denotes whether or not an object is emitting within the luminosity range of interest. Here we use distance and parallax interchangeably, and Kao & Shkolnik (submitted) provide the algebra for using either. In the analysis that we present in §4.3, we use parallaxes when available and distance estimates otherwise.

Kao & Shkolnik (submitted) describe how to calculate $\mathbb{P}(\sigma_{\text{rms}_\text{i}})$, $\mathbb{P}(\sigma_{\text{d}_\text{i}})$, and $\mathbb{P}(d_i)$, which are the probabilities that an object possesses the given observations/properties. These remain the same for unresolved binary systems. They additionally describe how to calculate $\mathbb{P}(L_{\nu,i} \geq L_{\text{thr,i}} \mid \sigma_{\text{rms}_\text{i}}, \sigma_{\text{d}_\text{i}}, d_i, e = 1)$ for single objects. To calculate this probability, an emitting object is also detectable, they integrate over the set of possible object distances. They also integrate over detectable object luminosities from an assumed luminosity distribution for emitting objects $\mathcal{P}(L_{\nu,\text{single}} \mid e = 1)$ within a luminosity range of interest $L_{\nu,\text{single}} \in [L_{\nu,\text{min}}, L_{\nu,\text{max}}]$:

$$\mathbb{P}(L_{\nu,i} \geq L_{\text{thr,i}} \mid \sigma_{\text{rms}_\text{i}}, \sigma_{\text{d}_\text{i}}, d_i, e = 1) = \int_0^{d_{\text{thr,max}_\text{i}}} \mathcal{P}(x_i \mid \sigma_{\text{d}_\text{i}}, d_i) \int_{L_{\text{thr,i}}}^{L_{\nu,\text{max}}} \mathcal{P}(L_{\nu,i} \mid e = 1) \quad dL_{\nu,i}\, dx_i \quad . \tag{2}$$

The only change required for applications to unresolved binary systems is replacing $\mathcal{P}(L_{\nu,\text{single}} \mid e = 1)$ with the luminosity distribution of unresolved binary systems given that the system is emitting, $\mathcal{P}(L_{\nu,\text{binary}} \mid e = 1)$. For the remainder of this section, we address $\mathcal{P}(L_{\nu,\text{binary}} \mid e = 1)$.

For single objects, $\mathcal{P}(L_{\nu,\text{single}} \mid e = 1)$ does not depend on the occurrence rate. Furthermore, it does not require any assumptions about how probability mass is distributed for $L_{\nu,\text{single}} \notin [L_{\nu,\text{min}}, L_{\nu,\text{max}}]$ outside of the luminosity range of interest.

However, for unresolved multi-object systems, we must consider the full luminosity distribution $\mathcal{P}(L_{\nu,\text{single}})$ for single objects. The occurrence rate now refers to that of unresolved binary systems $\theta_{\rm binary}$ rather than the individual components of binary systems. Consequently, the luminosity prior $\mathcal{P}(L_{\nu,\text{binary}} \mid e = 1)$ must refer to that of unresolved binary systems given that each system as a whole is emitting between the assumed luminosity range of interest. For comparisons to single-object systems, care must be taken to ensure an apples-to-apples comparison.

In particular, we must construct $\mathcal{P}(L_{\nu,\text{binary}} \mid e = 1)$ within the context of the luminosity distribution for single objects $\mathcal{P}(L_{\nu,\text{single}})$. This is because unresolved binaries emit when one or both of their components are emitting. Furthermore, they can satisfy the emission threshold even

if both components are individually too faint to meet the emission threshold. We discuss this additional caveat in §2.1. Thus, we must account for all cases.

The luminosity for an unresolved binary is equal to the summed luminosities of the a and b components such that $L_{\nu,\mathrm{binary}} = L_{\nu,a} + L_{\nu,b}$. We assume that the luminosities for the individual components each follow the distribution $\mathcal{P}(L_{\nu,\mathrm{single}})$, which gives the convolution

$$\mathcal{P}(L_{\nu,\mathrm{binary}}) = \begin{cases} \mathcal{P}(L_{\nu,\mathrm{single}}) * \mathcal{P}(L_{\nu,\mathrm{single}}) & , \ 0 \leq L_{\nu,\mathrm{binary}} \leq 2L_{\nu,\mathrm{max}} \\ 0 & , \ \text{otherwise} \quad . \end{cases} \tag{3}$$

Notice that this extends possible luminosities for $\mathcal{P}(L_{\nu,\mathrm{binary}})$ to higher luminosities. Accordingly, the binary luminosity range of interest for $e = 1$ becomes $L_{\nu,\mathrm{binary}} \in [L_{\nu,\mathrm{min}}, 2L_{\nu,\mathrm{max}}]$, where we remind the reader that $L_{\nu,\mathrm{max}}$ is the maximum luminosity for a single object. Here, the probability mass for $\mathcal{P}(L_{\nu,\mathrm{single}})$ is distributed such that the occurrence rate of quiescent radio emission for a single object, θ_{single}, is equal to the integrated probability mass between the minimum and maximum possible luminosities for a single object:

$$\int_{L_{\mathrm{min}}}^{L_{\mathrm{max}}} \mathcal{P}(L_{\nu,\mathrm{single}}) dL_{\nu,\mathrm{single}} = \theta_{\mathrm{single}} \tag{4}$$

The remaining probability mass $1 - \theta_{\mathrm{single}}$ is distributed over $L_{\nu,\mathrm{single}} \notin [L_{\nu,\mathrm{min}}, L_{\nu,\mathrm{max}}]$.

When we consider the case that both components are emitting, the distribution of probability mass $1 - \theta_{\mathrm{single}}$ outside of $L_{\nu,\mathrm{single}} \notin [L_{\nu,\mathrm{min}}, L_{\nu,\mathrm{max}}]$ becomes relevant. For instance, an individual object that is emitting at $L_{\nu,\mathrm{single}} = 0.8L_{\mathrm{min}}$ is not considered "emitting" in the single-object framework. In contrast, if both components in a binary are emitting at that luminosity, the binary luminosity $L_{\nu,\mathrm{binary}} = 1.6L_{\mathrm{min}}$ is within the binary luminosity range of interest. In §3, we discuss our choice for distributing the non-emitting probability mass $1 - \theta_{\mathrm{single}}$.

We can now re-write Eq. 1 to:

$$\mathbb{P}(D \mid \theta_{\mathcal{B}} = \Theta) = \prod_{i=1}^{N} \mathbb{P}(\sigma_{\mathrm{rms_i}})\, \mathbb{P}(\sigma_{\mathrm{d_i}})\, \mathbb{P}(d_i)\, \mathbb{P}(\mathcal{B}) \times \begin{cases} \Theta\, \mathbb{P}(L_{\nu,i} \geq L_{\mathrm{thr,i}} \mid \theta_{\mathcal{B}} = \Theta, \mathcal{B}, \sigma_{\mathrm{rms_i}}, \sigma_{\mathrm{d_i}}, d_i, e = 1) & , \ \mathrm{detect}_i = 1 \\ 1 - \Theta\, \mathbb{P}(L_{\nu,i} \geq L_{\mathrm{thr,i}} \mid \theta_{\mathcal{B}} = \Theta, \mathcal{B}, \sigma_{\mathrm{rms_i}}, \sigma_{\mathrm{d_i}}, d_i, e = 1) & , \ \mathrm{detect}_i = 0 \quad . \end{cases} \tag{5}$$

Here, we have also added the multiplicative term $\mathbb{P}(\mathcal{B})$, or the probability that an object is in a given population p, where $\mathcal{B} \in [\mathrm{single}, \mathrm{binary}]$. This allows us to condition on the appropriate luminosity distribution for each population. Notice that the probability that an emitting object's radio luminosity is detectable now depends on the assumed binary radio occurrence rate, and by implication, the single-object radio occurrence rate.

2.1 Constructing a predicted binary occurrence rate $\theta_{\mathrm{predict}}$ from the single-object occurrence rate θ_{single}

To compare single objects to binary systems, we must consider the appropriate change of variables from the single-object occurrence rate θ_{single} to a predicted binary occurrence rate $\theta_{\mathrm{predict}}$. We can then compare the binary occurrence rate θ_{binary} to $\theta_{\mathrm{predict}}$. In Eq. 5, θ_{binary} refers to the occurrence rate of binaries in which the sum of both components fall into the binary luminosity range of interest such that

$$\theta_{\mathrm{binary}} = \mathbb{P}((L_a + L_b \geq L_{\mathrm{min}}) \cap (L_a + L_b \leq L_{\mathrm{max}})) \quad . \tag{6}$$

We choose an appropriate L_{max} such that the single-object luminosity prior takes the form

$$\mathcal{P}(L_{\nu,\mathrm{single}}) = \begin{cases} 0 & , \quad L_{\nu,\mathrm{single}} > L_{\nu,\mathrm{max}} \\ \theta_{\mathrm{single}}\, \mathcal{F}_1(L_{\nu,\mathrm{single}}) & , \quad L_{\nu,\mathrm{single}} \in [L_{\nu,\mathrm{min}}, L_{\nu,\mathrm{max}}] \\ (1 - \theta_{\mathrm{single}})\, \mathcal{F}_2(L_{\nu,\mathrm{single}}) & , \quad L_{\nu,\mathrm{single}} < L_{\nu,\mathrm{min}} \quad , \end{cases} \tag{7}$$

where we discuss $L_{\nu,\mathrm{max}}$ in §3.2, and $\mathcal{F}_1(L_{\nu,\mathrm{single}})$ and $\mathcal{F}_2(L_{\nu,\mathrm{single}})$ are normalized density functions that depend on $L_{\nu,\mathrm{single}}$. This generalized form meets the condition defined in Eq. 4 and gives us the freedom to examine how distributions with different shapes impact the final calculated binary occurrence rate. For instance, a situation where objects are either "on" or "off" can be described by a luminosity prior where the probability mass for $L_{\nu,\mathrm{single}} < L_{\nu,\mathrm{min}}$ is concentrated as a delta function at $L_{\nu,\mathrm{single}} = 0$. This may be the case for non-thermal quiescent radio emission but not for thermal emission. Eq. 6 then simplifies to $\theta_{\mathrm{binary}} = \mathbb{P}(L_a + L_b \geq L_{\mathrm{min}})$.

We use Eq. 6 to construct $\theta_{\mathrm{predict}}$ by assuming that binarity does not affect the radio occurrence rate of individual components. We also assume that the luminosities of each binary's individual components are drawn from the single-object luminosity distribution $\mathcal{P}(L_{\nu,\mathrm{single}})$. In §3, we examine this latter assumption. We can then account for all combinations of $L_a + L_b$ by invoking the law of total probability and integrating

$$\theta_{\mathrm{predict}} = \int_0^{L_{\mathrm{max}}} \mathbb{P}(L_a + k \geq L_{\mathrm{min}}) \mathcal{P}(L_b = k)\, dk \tag{8}$$

$$= \int_0^{L_{\mathrm{max}}} \mathbb{P}(L_a \geq L_{\mathrm{min}} - k) \mathcal{P}(L_b = k)\, dk \quad , \tag{9}$$

where $\mathcal{P}(L_b = k)$ is the probability density distribution that the b component has a luminosity equal to k. This distribution is our chosen single-object luminosity distribution, such that $\mathcal{P}(L_b = k) = \mathcal{P}(L_{\nu,\mathrm{single}} = k)$, and it gives the relationship between θ_{single} and $\theta_{\mathrm{predict}}$. Eq. 9 simplifies to

$$\theta_{\mathrm{binary}} = C(\theta_{\mathrm{single}}) + 1 - (1 - \theta_{\mathrm{single}})^2 \quad , \tag{10}$$

where $C(\theta_{\mathrm{single}})$ is a correction factor. When the non-emitting probability mass is a delta function at zero, $C(\theta_{\mathrm{single}}) = 0$ because the radio

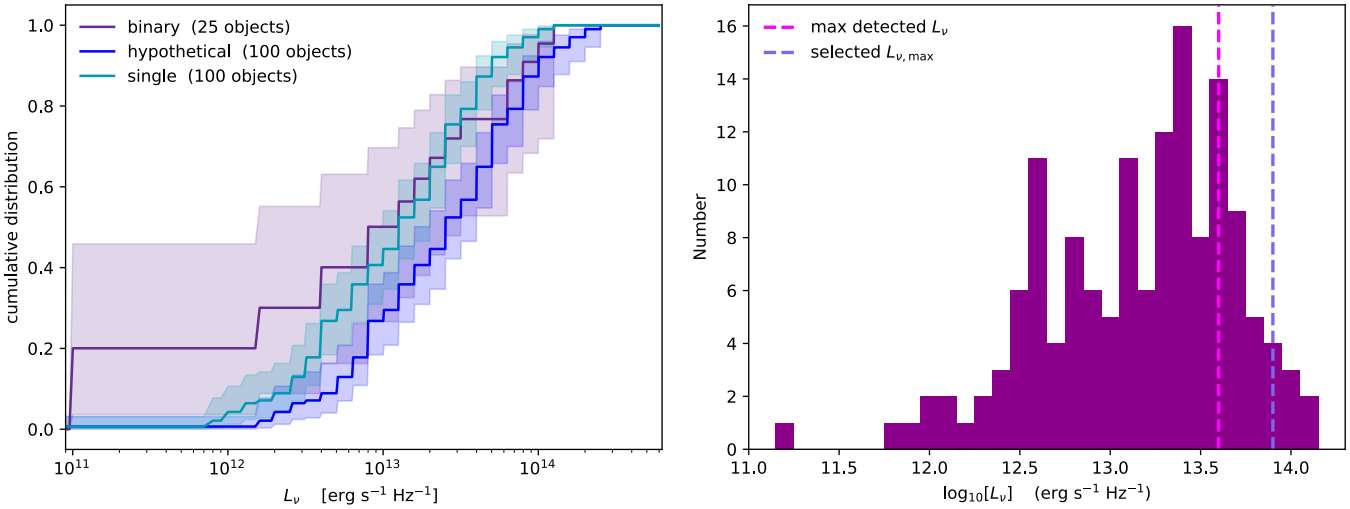

Figure 1. —Left: Empirical cumulative distribution function for all observed single objects that meet the data inclusion criteria of Kao & Shkolnik (submitted) (teal), a hypothetical set of binaries that have $L_\nu = 2L_{\nu,\mathrm{single}}$ (blue), and detected binary systems (purple) within 35 pc. Shaded regions are 95% confidence intervals. Detected objects with more than one measurement are represented with their median value. Distributions and confidence intervals are the mean distributions from 1000 trials in which we randomly draw single objects to match the spectral type distribution of the binary systems. The low luminosity end of the binary distribution is consistent with the single-object distribution, and the high luminosity end is consistent with the hypothetical distribution. — Right: Histogram of 4σ luminosity limits for undetected single objects with 3σ distances within 35 pc. 85% of single-object observations had luminosity limits that would have been sufficient to detect the brightest quiescent radio emission observed in single objects.

occurrence rate for binaries is one minus the probability that neither component is emitting. When the mass is not distributed as a delta function, $C(\theta_{\mathrm{single}})$ is positive and accounts for the additional pairs of objects that may be too faint individually to fall above $L_{\nu,\mathrm{single}} \geq L_{\mathrm{min}}$ but together are luminous enough to fall above $L_{\nu,\mathrm{binary}} \geq L_{\mathrm{min}}$. From Eq. 10, we expect that unresolved binaries are more likely to emit radio emission than their single counterparts when all else is equal.

3 DEFINING THE LUMINOSITY DISTRIBUTION $\mathcal{P}(L_{\nu,\mathrm{single}})$

3.1 Do individual binary components follow the same luminosity distribution as single objects?

As described in §2, self-consistent comparisons between single and binary systems require a binary luminosity prior constructed from that of single objects. For our analysis, we do not condition the underlying single-object luminosity distribution $\mathcal{P}(L_{\nu,\mathrm{single}})$ on binarity. One consequence of our treatment is that we expect unresolved binary systems to be more luminous on average than single objects when all else is equal. Indeed, the data seem to support this assumption, with mean quiescent radio luminosities for detected binaries brighter than that of detected single objects (Kao & Pineda accepted).

In Figure 1, we further justify our assumption by examining empirical cumulative distribution functions (ECDF) and 95% confidence intervals using the Kaplan-Meier estimator for observed single objects, binaries, and a hypothetical set of binaries constructed with our single-object sample. §4.1 describes our data. The Kaplan-Meier estimator is a non-parametric statistic used in survival analysis (Kaplan & Meier 1958; Lee & Wang 2003), which allows one to incorporate non-detections and limits within cumulative distribution functions. In our case, it estimates the probability that the observed object's luminosity is less than some value.

We use the full set of compiled observations from the literature for objects that are within 35 pc, including non-detections. This distance cutoff is consistent with all detected objects, and it includes 151 and 25 single and binary systems, respectively, or 84% and 86% of observed systems. Figure 1 shows a histogram of 4σ sensitivity limits for all undetected single object systems with radio observations that have 3σ distances within 35 pc. For objects with repeated observations, we use the median measured luminosity. We treat binaries as unresolved systems by combining the reported luminosities for 2MASS J07464256+2000321AB, for which resolved observations using the Very Long Baseline Array show both components are emitting (Zhang et al. 2020). Finally, each undetected object is represented only once as an upper limit corresponding to the most sensitive observation that is available in the literature for that object.

We account for upper limits by treating non-detections as left-censored data. The estimator makes the fundamental assumption that all objects in the given data set are emitting non-thermal radio emission, even if it is not detectable. However, it is important to note that this assumption may not be true, since some undetected objects may not be emitting non-thermal radio emission at all. Kao & Shkolnik (submitted) find that ~15–20% of objects may not be emitting non-thermal radio emission brighter than $10^{11.7}$ erg s^{-1} Hz^{-1}, so future observations at higher sensitivities may yield a significant number of upper limits at lower luminosities. In this case, we expect a significant portion of the probability mass in the ECDFs for the single and hypothetical populations to shift leftward to lower luminosities.

For our hypothetical set of binaries, we randomly draw objects from the single-object sample to match the spectral type distribution of the individual components in the binary sample. We repeat this trial 1000 times and show the mean distribution and 95% confidence interval in Figure 1. We find that the low luminosity end of the binary distribution is consistent with the single-object distribution and the high luminosity end is consistent with the hypothetical binary distribution. Even though Kao & Pineda (accepted) observed that the highest luminosities observed in single ultracool dwarfs could not account for the most luminous detected binaries, controlling for spectral type distributions seems to show that single and binary objects do not have statistically different underlying luminosity functions. This further grounds our choice not to condition the underlying single-object luminosity distribution $\mathcal{P}(L_{\nu,\mathrm{single}})$ on binarity.

3.2 Choosing a self-consistent luminosity distribution

To assess if binaries have elevated radio occurrence rates relative to *analogous* single objects, we must use a luminosity distribution that is consistent for both the single and binary populations. Kao & Shkolnik (submitted) adopted a luminosity prior with minimum and maximum single-object luminosities that correspond to those observed for the known population of radio-bright ultracool dwarfs at our frequencies of interest. Although we show in §3 that the underlying luminosity distribution for the individual components of binary systems is statistically indistinguishable from that of observed objects, Kao & Pineda (accepted) show that some detected binaries can be more luminous than summed luminosities from the most luminous detected single objects. Thus, we cannot adopt the same minimum and maximum observed single-object luminosities that Kao & Shkolnik (submitted) used. Instead, we must revise the luminosity range.

First, we choose $L_{\nu,\mathrm{max}}$ such that all empirical detections of single objects have $L_{\nu,\mathrm{single}} \leq L_{\nu,\mathrm{max}}$ and it reasonably accounts for detection limits. Twice the brightest reported quiescent radio luminosity for single objects corresponds to $[L_\nu] \sim 13.9$ erg s^{-1} Hz^{-1}, but the M7+M7 binary 2MASS J13142039+1320011 (also known as NLTT 33370 AB) has luminosities up to $[L_\nu] \sim 14.6$ erg s^{-1} Hz^{-1} (McLean et al. 2011). Surprisingly, resolved observations demonstrate that only one component of this system is emitting (Forbrich et al. 2016). As Kao & Pineda (accepted) note, this suggests the possibility that individual components in binary systems may be overluminous compared to single-object systems. However, radio luminosities for this system can differ by greater than a factor of 2 (Williams et al. 2015a; Forbrich et al. 2016), and some portion of its radio emission has been attributed to gyrosynchrotron flares (Williams et al. 2015a).

Since the radio luminosity of 2MASS J13142039+1320011 may not trace solely quiescent radio emission, we turn to the next most luminous binary system, 2MASS J13153094-2649513AB. This L3.5+T7 binary has $[L_\nu] \sim 14.2$ erg s^{-1} Hz^{-1} (Burgasser et al. 2013a), which is still overly luminous compared to the brightest single objects.

Thus, for this calculation, we choose $[L_{\nu,\mathrm{max}}] = 13.9$ for single objects. This upper limit, revised from 13.6, is consistent with reported binary luminosities and it includes 97% of luminosity limits for single objects within 35 pc. Finally, it corresponds to twice the maximum quiescent radio luminosity of detected ultracool dwarfs, which is consistent with observed levels of variability in ultracool dwarf quiescent radio emission (Kao & Shkolnik submitted, and references therein). The one outlier is the L2.5 dwarf 2MASS J05233822-1403022, which Antonova et al. (2007) report can vary by a factor of ~5 from ≤45 to 230±17 μJy with no evidence of short-duration flares during 2-hr observing blocks. Although the low circular polarization of this object rules out coherent aurorae, non-auroral flares at both radio and optical frequencies can persist for at least several hours (e.g. Villadsen & Hallinan 2019; Paudel et al. 2018b). This outlier object has been excluded from the single-object sample by Kao & Shkolnik (submitted) on the basis of the uncertain nature of its radio emission, similar to our reasoning for excluding the binary 2MASS J09522188-1924319.

Following Kao & Shkolnik (submitted), we assume two luminosity distributions for our calculations, which we show in Figure 2:

- **Uniform$_{e=1}$:** Emitting single objects have radio luminosities that are uniformly distributed between $L_{\nu,\mathrm{single}} \in [L_{\nu,\mathrm{min}} = 11.7, L_{\nu,\mathrm{max}} = 13.9]$. Here, $L_{\nu,\mathrm{min}}$ corresponds to the minimum detected radio luminosity for single ultracool dwarfs, and our chosen $L_{\nu,\mathrm{max}}$ provides an upper bound for existing detection measurements. By including repeat observations of the same object, we can account for the intrinsic variability of individual objects. Calculations that use this luminosity distribution assume that our only prior knowledge about the luminosity distribution are the minimum and maximum values, as is the case with the existing limited data.
- **KM$_{e=1}$:** Alternatively, we can assume that emitting objects follow the same luminosity distribution of *all measured detections*. We construct this prior by fitting the Kaplan-Meier ECDF of emitting single objects with a piece-wise linear function (Figure 2) and differentiating the fitted function. This prior also accounts for intrinsic variability in individual objects, but it may be skewed from the true underlying luminosity distribution due to the non-uniformity of repeated observations and small sample size (33 measurements). The KM probability density distribution initially extends only to $[L_\nu] = 13.6$ erg s^{-1} Hz^{-1}, but it is characterized by two concatenated uniform distributions (Figure 2). Accordingly, we extend the luminosity distribution to our chosen maximum limit $[L_\nu] = 13.9$ erg s^{-1} Hz^{-1} and re-normalize.

Figure 2 shows our chosen luminosity priors for $\mathcal{P}(L_{\nu,\mathrm{single}} \mid e = 1)$. Using the same luminosity priors for both the single and binary populations controls for luminosity differences between single and binary populations and allows us to ask whether binaries have elevated occurrence rates relative to analogous single objects.

As discussed in §2, the probability mass outside of the luminosity prior for emitting single objects ($e = 1$) impacts the probability distribution for the binary luminosities. The single-object radio occurrence rate θ_{single} corresponds to the probability that an object is emitting within the assumed luminosity bounds $[L_{\nu,\mathrm{single}}] \in [11.7, 13.9]$ erg s^{-1} Hz^{-1}. Thus, we attribute θ_{single} of the probability mass for $\mathcal{P}(L_{\nu,\mathrm{single}})$ within these assumed bounds. Finally, we must decide how to distribute the rest of the probability mass $(1 - \theta_{\mathrm{single}})$ between $[L_{\nu,\mathrm{single}}] \in [0, 11.7)$ erg s^{-1} Hz^{-1}.

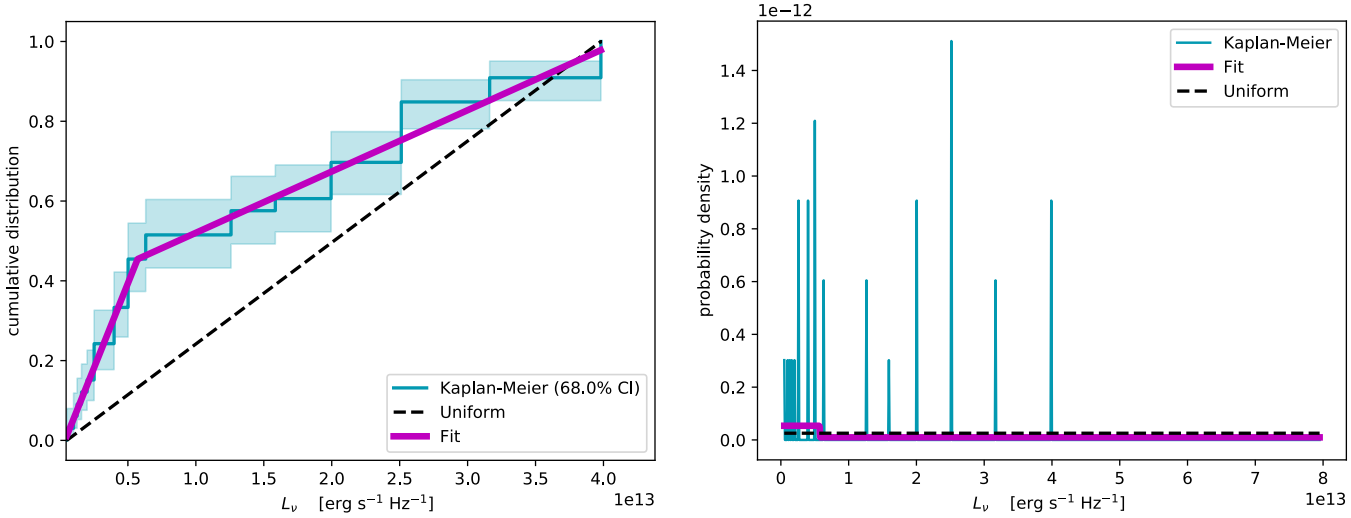

Figure 2. Left: The empirical cumulative distribution function for L_ν for all radio detections of single ultracool dwarfs, calculated using the Kaplan-Meier estimator (teal). Right: The probability density distribution calculated from the cumulative distribution function of single-objects, with the fitted piece-wise linear prior $\mathcal{P}(L_{\nu,\mathrm{single}} \mid e = 1)$ (magenta) and a uniform prior (black) extended to the full luminosity range that we choose and renormalized. We run calculations for both the distributions.

For this work, we examine the case where $(1 - \theta)$ of the mass is located at $L_{\nu,\mathrm{single}} = 0$. This simplest case equivalently assumes that single ultracool dwarfs only emit radio emission between $[L_{\nu,\mathrm{single}}] \in [11.7, 13.9]$ erg s^{-1} Hz^{-1}.

Our assumption is motivated by the fact that a number of factors can contribute to a lack of quiescent radio emission from a given ultracool dwarf. Such factors include but are not limited to the absence of a plasma source, magnetic fields that may not be sufficient in size or strength to confine the plasma, or the absence of a mechanism that can accelerate magnetospheric plasma to the mildly relativistic energies required for gyrosynchrotron emission. Indeed, planets demonstrate that not all objects meet the necessary conditions for producing quiescent radio emission. For example, the magnetized planets in our solar system (Mercury, Earth, Jupiter, Saturn, Uranus, Neptune) are “on", whereas the unmagnetized solar system planets (Mars, Venus) are “off" (Khurana et al. 2004; Bolton et al. 2004; Girard et al. 2016; Mauk & Fox 2010; Kellermann 1970; Basharinov et al. 1974; Ganushkina et al. 2011). Similarly, deep observations of the nearest brown dwarf binary system Luhman 16AB (2.02±0.15 pc, Luhman 2013) and the Y dwarf WISE J085510.83-071442.5 (2.23±0.16 pc, Tinney et al. 2014) rule out radio emission down to $[L_\nu] \leq 11.0$ and ≤ 11.2 erg s^{-1} Hz^{-1}, respectively, at 4σ significance (Osten et al. 2015; Kao et al. 2019).

Assuming that ultracool dwarfs emit only within the bounds $[L_{\nu,\mathrm{single}}] \in [11.7, 13.9]$ erg s^{-1} Hz^{-1} captures the observed range of detected ultracool dwarf quiescent radio luminosities. However, the existing set of detected objects may not fully capture the faint end of the ultracool dwarf luminosity distribution. Thus, we also include calculations for a hypothetical $\mathcal{P}(L_{\nu,\mathrm{single}})$ with $[L_{\nu,\mathrm{single}}] \in [9.8, 13.9]$ erg s^{-1} Hz^{-1}. Existing quiescent radio luminosities span 1.9 dex, and the revised lower limit reflects an additional 1.9 dex.

4 APPLYING THE FRAMEWORK

4.1 Data

To compare the radio occurrence rates of binary systems to single objects, we use the compilations of single objects in Kao & Shkolnik (submitted). This set includes 82 ultracool M dwarfs, 74 L dwarfs, and 23 T/Y dwarfs. We also use all available measurements of *detected* quiescent radio emission from binary ultracool dwarfs, compiled in Table 4 of Kao & Pineda (accepted). To define the luminosity priors that we assume for our occurrence rate calculations in §3.2, we use the combined dataset of all detected quiescent radio emission measurements for single objects and binaries.

Finally, we performed a literature search to compile a list of all radio observations, *including non-detections*, of ultracool dwarf binaries with individual components that have spectral type ≥M7. For objects with multiple recorded observations, we follow the data inclusion policy described in Kao & Shkolnik (submitted) to produce a data set that represents observations that are independent from each other. In this data set, each object is represented only once. For each non-detected object, we select its most sensitive observation. For each detected object, we select the detection with the lowest rms noise. Furthermore, the flux densities that we list correspond to quiescent emission and exclude contributions from identified flares. This latter dataset serves as the input dataset for our occurrence rate calculations in §4.

Our binary sample contains 28 systems, summarized in Table 1. For binaries with reported radio emission for separate components, we choose the higher rms value to be conservative and designate the binary as detected if at least one component was detected. We include only binary systems for which both components are ultracool dwarfs and exclude triples except for hierarchical systems in which observations resolve the binary. For the triple system 2MASS J12560183-1257276, we include the primary component, an M7.5+M7.5 close-in binary system (Stone

Table 1. Radio Observations of Multi-object Ultracool Dwarf Systems from the Literature

Object Name	SpT	π (mas)	d (pc)	F_ν (μJy)	ref	Note
2MASS J00244419-2708242	M6+M8.5+M9	132.3 ± 11.4	7.6 ± 0.7	<111.0	41 37 57 44	a
2MASS J00275592+2219328	M7+M8	69.2 ± 0.9	14.5 ± 0.2	323 ± 14	24 24 24 47	b
2MASS J04291842-3123568	M7.5+L1	59.3757 ± 0.2018	16.8 ± 0.06	<48	53 54 28 6	
2MASS J09522188-1924319	M7	34.5193 ± 0.1511	29.0 ± 0.13	233 ± 15	45 50 28 47	c
2MASS J11214924-1313084	M8.5+L7.5	69.4903 ± 0.176	14.4 ± 0.04	<102	3 24 28 47	
2MASS J12073346-3932539	M8+L5	19.1 ± 0.4	52.4 ± 1.1	<29	31 7 23 49	
2MASS J12560183-1257276 Aab	M7.5+M7.5	78.8 ± 6.4	12.7 ± 1.0	60 ± 3	29 29 29 33	d
2MASS J17072343-0558249	M9+L3		7.0 ± 1.0	<48	51 46 26 6	
2MASS J22000201-3038327	M8+L0	41 ± 4	24.4 ± 2.4	<78	26 12 42 47	
2MASS J22062280-2047058	M8.0+M8.5	35.8 ± 1	27.9 ± 0.8	<84	20 24 24 47	
GJ 569 Bab	M8.5+M9	93.814 ± 0.724	10.7 ± 0.1	<30	38 24 28 6	e
WISE J072003.20-084651.2	M9+T5	$147.1^{+1.1}_{-1.2}$	$6.8^{+0.05}_{-0.06}$	15 ± 3	18 25 25 19	
2MASS J00043484-4044058	L5+L5	82.0946 ± 0.3768	12.2 ± 0.1	100 ± 8.3	51 32 28 44	f
2MASS J02052940-1159296	L5+L8+T0	50.6 ± 1.5	19.8 ± 0.6	<30	10 10 27 6	
2MASS J03105986+1648155	L9+L9	36.9 ± 3.4	27.1 ± 2.5	<10.8	35 56 55 52	
2MASS J04234858-0414035	L6.5+T2	67.8584 ± 1.5052	14.7 ± 0.3	54.1 ± 2.2	23 24 28 34	
2MASS J07003664+3157266	L3+L6.5	88.279 ± 0.3479	11.33 ± 0.04	<42	23 24 28 1	
2MASS J07464256+2000321 A	L0	80.9 ± 0.8	12.4 ± 0.1	71 ± 12	9 24 24 58	
2MASS J07464256+2000321 B	L1.5	80.9 ± 0.8	12.4 ± 0.1	128 ± 14	9 24 24 58	
2MASS J10491891-5319100	L7.5+T0.5	496 ± 37	2.0 ± 0.2	<15	17 40 43 48	
2MASS J12281523-1547342	L5.5+L5.5	48 ± 1.7	20.8 ± 0.7	<87	23 21 24 5	g
2MASS J13054019-2541059	L2+L3.5	53.8492 ± 0.7107	18.6 ± 0.2	<27.6	36 24 28 39	
2MASS J13153094-2649513	L3.5+T7	53.8729 ± 1.1265	18.6 ± 0.4	370 ± 50	14 15 28 16	
2MASS J14413716-0945590	L1+L1	31.6439 ± 1.0131	31.6 ± 1.0	<84	51 8 28 47	
2MASS J17114573+2232044	L5.0+T5.5	33.11 ± 4.81	30.2 ± 4.4	<11.4	13 4 27 52	
2MASS J17281150+3948593	L5+L6.5	36.4 ± 0.6	27.5 ± 0.5	<54	30 24 24 6	
2MASS J22521073-1730134	L4.5+T3.5	59.1461 ± 0.8244	16.9 ± 0.2	<30	23 24 28 6	
2MASS J15344984-2952274	T4.5+T5	63 ± 1.1	15.9 ± 0.3	<63	23 24 24 6	
2MASS J22041052-5646577 A	T1+T6	275.79 ± 0.69	3.63 ± 0.01	<79.2	11 22 43 2	h
2MASS J22041052-5646577 B	T1+T6	275.79 ± 0.69	3.63 ± 0.01	<79.2	11 22 43 2	

Note – Distances calculated from parallaxes are provided for the reader's convenience but are truncated to three significant figures in the interest of space. We report upper limits or flux densities as presented in the radio observation references and define detected = 1 if $F_\nu \geq 4.0$ to remain consistent with our occurrence rate calculation. Reference order: SpT, d, F_ν.

[a] We do not include 2MASS J00244419-2708242 in the binary calculation because the ATCA 6A configuration cannot resolve this triple system.

[b] McLean et al. (2012) list 2MASS J00275592+2219328 as LP 349-25 B, but the primary and secondary components of this binary are unresolved by the VLA. Thus, we list this observation for both components.

[c] Reid et al. (2002) report that 2MASS J09522188-1924319 is an unresolved double-lined spectroscopic binary, but Guenther & Wuchterl (2003) observed only a single line. We exclude this system due to the possibility that its detected radio emission may be flaring rather than quiescent emission (McLean et al. 2012).

[d] The discovery that the primary in the 2MASS J12560183-1257276 AB system is actually an equal-mass binary (Stone et al. 2016) suggests that this system may be as far as 17.1 ± 2.5 pc rather than the 12.7 ± 1.0 pc reported by Gauza et al. (2015). The wide ≥ 102 ± 9 AU separation between the primary and secondary components (Gauza et al. 2015) is easily resolved in all observations and precludes magnetic interactions between components, so we include 2MASS J12560183-1257276 Aab in the binary sample. item[e] GJ 569 Bab is a companion to an M3 primary that is separated by ∼53 AU. This corresponds to ∼5" (Forrest et al. 1988) and is resolved by the VLA. The wide separation precludes magnetic interactions between components, so we include GJ 569 Bab in the binary sample.

[f] 2MASS J00043484-4044058 (GJ 1001) is a triple system, in which the M4 primary is separated by ∼180 pc from the L5+L5 binary secondary (Golimowski et al. 2004). The observation reported here is for the binary component of the triple. This distance is easily resolved, so we include this observation in the binary sample. Golimowski et al. (2004) do not give error estimates for their measured angular separation.

[g] Dupuy & Liu (2017) note that the orbit fit for 2MASS J12281523-1547342 is of questionable quality.

[h] 2MASS J22041052-5646577 is also known as ϵ Ind Bab.

References – (1) Antonova et al. (2013) ; (2) Audard et al. (2005) ; (3) Bardalez Gagliuffi et al. (2014) ; (4) Bardalez Gagliuffi et al. (2015) ; (5) Berger (2002) ; (6) Berger (2006) ; (7) Blunt et al. (2017) ; (8) Bouy et al. (2003) ; (9) Bouy et al. (2004) ; (10) Bouy et al. (2005) ; (11) Burgasser et al. (2005) ; (12) Burgasser & McElwain (2006) ; (13) Burgasser et al. (2010) ; (14) Burgasser et al. (2011b) ; (15) Burgasser et al. (2011a) ; (16) Burgasser et al. (2013a) ; (17) Burgasser et al. (2013b) ; (18) Burgasser et al. (2015b) ; (19) Burgasser et al. (2015a) ; (20) Deshpande et al. (2012) ; (21) Dieterich et al. (2014) ; (22) Dieterich et al. (2018) ; (23) Dupuy & Liu (2012) ; (24) Dupuy & Liu (2017) ; (25) Dupuy et al. (2019) ; (26) Faherty et al. (2009) ; (27) Faherty et al. (2012) ; (28) Gaia Collaboration (2018) ; (29) Gauza et al. (2015) ; (30) Gelino et al. (2014) ; (31) Gizis (2002) ; (32) Golimowski et al. (2004) ; (33) Guirado et al. (2018) ; (34) Kao et al. (2016) ; (35) Kirkpatrick et al. (2000) ; (36) Koen (2013) ; (37) Köhler et al. (2012) ; (38) Konopacky et al. (2010) ; (39) Krishnamurthi et al. (1999) ; (40) Lazorenko & Sahlmann (2018) ; (41) Leinert et al. (2000) ; (42) Liu et al. (2016) ; (43) Luhman (2013) ; (44) Lynch et al. (2016) ; (45) McCaughrean et al. (2002) ; (46) McElwain & Burgasser (2006) ; (47) McLean et al. (2012) ; (48) Osten et al. (2015) ; (49) Osten & Jayawardhana (2006) ; (50) Reid et al. (2002) ; (51) Reid et al. (2008) ; (52) Richey-Yowell et al. (2020) ; (53) Schmidt et al. (2007) ; (54) Siegler et al. (2005) ; (55) Smart et al. (2013) ; (56) Stumpf et al. (2010) ; (57) Weinberger et al. (2016) ; (58) Zhang et al. (2020)

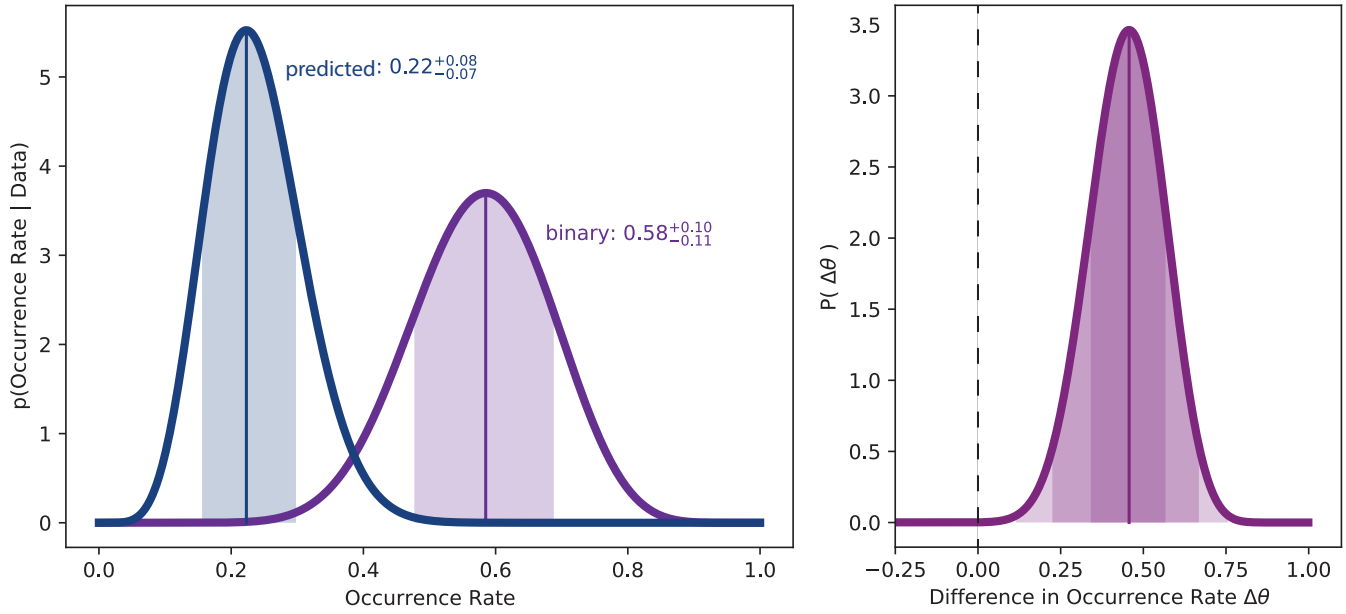

Figure 3. Calculations comparing binary to single-object systems using the full set of data available in the literature and assuming a uniform luminosity prior between $L_{\nu,\mathrm{single}} \in [11.7, 13.9]$.
— Left: Occurrence rate distributions of quiescent radio emission in ultracool dwarf binaries (purple) and the predicted occurrence rate distribution for binaries from single objects, where $\theta_{\mathrm{predicted}} = 1 - (1 - \theta_{\mathrm{single}})^2$ (teal). Shaded regions correspond to the 68.3% credible intervals. Individual components in binary systems are more likely to emit radio emission than their single counterparts. — Right: Probability density distribution for the difference in occurrence rates $\Delta\theta = \theta_{\mathrm{binary}} - \theta_{\mathrm{predict}}$ between binaries and predictions from single objects. Shaded regions correspond to 68.3%, 95.5% and 99.7% credible intervals. Existing data rule out the null hypothesis that binarity does not affect quiescent radio occurrence rates.

et al. 2016). We exclude the L7.0 secondary component due to its wide $\geq 102 \pm 9$ AU separation (Gauza et al. 2015), which is more than ~30 times the separation between the Sun and Jupiter and is easily resolved in all observations. Given its large separation, we include it in the single-object sample instead. Similarly, we include the binary system 2MASS J00043484-4044058 BC (GJ 1001 BC) and ϵ Ind Bab. These systems are part of widely-separated triple systems in which the primary components are separated from the secondary binary systems by ~180 AU (18″, Golimowski et al. 2004) and ~1459 AU (402″, Scholz et al. 2003). Finally, we also include GJ 564 BC. Although it resides in a triple system, the primary component is a solar analog at a distance of ~47 AU (Potter et al. 2002; Dupuy et al. 2009). This separation is not resolvable by the VLA for our observations, but solar radio emission from 4–8 GHz during solar maximum at this object's distance is not detectable by the VLA (Villadsen et al. 2014). Since the primary components of these systems are not ultracool dwarfs and are M4, K5V, and G2V stars, respectively, we do not include the primaries in the single sample.

We exclude from our sample LP 415-20 because of compelling evidence that the primary component of this system may in fact be unresolved ultracool dwarf binaries (Dupuy & Liu 2017). The primary is not resolvable from its secondary. We additionally exclude GJ 569 Bab, which is in a triple and separated from its M3 primary by ~50 AU (5″, Forrest et al. 1988). Although Berger (2006) do not report the observation date, VLA configuration, or observing frequency for this target, we surmise from an archive search that this target was observed during VLA B configuration at C band (Project Code AB1179, PI Bower). The separation between GJ 569 Bab and its primary is resolvable by the VLA for this observation. However, the stellar wind properties of M dwarfs are not well known, so we cannot be confident that GJ 569 Bab remains largely uninfluenced by its primary star at this separation. Finally, we exclude the M7+M7 binary 2MASS J09522188-1924319 due to the possibility that the radio emission detected from this object may be flaring rather than quiescent emission. McLean et al. (2012) detected 233 ± 15 μJy emission from this object, which corresponds to $[L_\nu] = 14.4$. However, they reported that followup observations at 4.96 and 8.46 GHz after the initial detection did not yield a detection to a limit of 69 μJy, or a factor of 2.4 below the original detection. They concluded that the initial detection was likely a flare or that 2MASS J09522188-1924319 exhibits long-term variability.

4.2 Analysis

To assess if binaries have an observed quiescent radio occurrence rate that is consistent with that of analogous single-objects, we compare occurrence rate distributions for two populations in Figure 3: the set of observed binaries, and a hypothetical set of constructed binaries.

For the hypothetical set of binaries, we randomly draw single-object systems without replacement to match the M, L, and T dwarf distribution of the individual components in the binary sample. The number of observed T dwarf systems limits the sizes of our drawn samples to 112 objects. We account for different possible combinations of single-object systems by repeating this procedure 1000 times and calculating the

probability density distribution of the occurrence rate for each trial using the single-object framework defined in Kao & Shkolnik (submitted). In other words, this occurrence rate reflects the occurrence rate that one would observe if each binary were split into its individual components.

We then take the mean distribution for single objects $\mathcal{P}(\theta_{\rm single})$ and transform it to a *predicted* distribution for our hypothetical binaries $\mathcal{P}(\theta_{\rm predict})$ by ensuring that

$$\int_{\theta_{\rm single,1}}^{\theta_{\rm single,2}} \mathcal{P}(\theta_{\rm single}) d\theta_{\rm single} = \int_{\theta_{\rm predict,1}}^{\theta_{\rm predict,2}} \mathcal{P}(\theta_{\rm predict}) d\theta_{\rm predict} \quad ,$$

which is the standard transformation for random variables. Here, $\theta_{\rm predict} = 1 - (1 - \theta_{\rm single})^2$ (Eq. 10). We compare $\mathcal{P}(\theta_{\rm predicted})$ to the actual calculated binary radio occurrence rate distribution $\mathcal{P}(\theta_{\rm binary})$ in Figure 3.

Finally, we also calculate the probability density distribution for differences in occurrence rates $\Delta\theta$ between predicted and actual binary systems, where

$$\mathcal{P}(\Delta\theta) = \int_{-1}^{1} \mathcal{P}(\theta_{\rm predict}) \mathcal{P}(\theta_{\rm binary} = \theta_{\rm predict} + \Delta\theta)\, d\theta_{\rm predict} \quad . \tag{11}$$

We can then calculate the probability that the binary radio occurrence rate exceeds the predicted occurrence rate by integrating

$$\mathbb{P}(\theta_{\rm binary} > \theta_{\rm predict}) = \int_{0}^{1} \mathcal{P}(\Delta\theta)\, d\Delta\theta \quad . \tag{12}$$

4.3 Results: Occurrence rate of binary systems compared to predictions from single objects

In Figure 3, we show that binary ultracool dwarf systems have an elevated radio occurrence rate compared to the rate predicted from their single counterparts. This figure uses the full set of objects that have been observed at radio frequencies and assumes that $[L_{\nu,\rm single}] \in [11.7, 13.9]$ erg s^{-1} Hz^{-1}.

We find that the quiescent occurrence rate for the binary sample is 58^{+10}_{-11}%. For comparison, the predicted binary occurrence rate from single-object systems with the same spectral type distribution as our binary systems is 22^{+8}_{-7}%. Quoted uncertainties correspond to 68.3% credible intervals.

Additionally, we find that the radio occurrence rate of binaries exceeds the predicted rate from single objects with probability $\mathbb{P}(\theta_{\rm binary} > \theta_{\rm predict}) = 100$%. We conclusively rule out the null hypothesis and further explore implications for the observed binary enhancement of radio occurrence rates in §5.

We find that binarity may enhance the ultracool dwarf quiescent radio occurrence rate even when we exclude objects from Kao et al. (2016). This targeted study selected objects with likely markers of auroral magnetic activity at other wavelengths such as Hα emission and infrared variability. These selection criteria resulted in a very high detection rate (80%) compared to the 5–10% detection rate in the literature (e.g. Route & Wolszczan 2016b; Richey-Yowell et al. 2020) that is consistent with that of volume-limited surveys (Antonova et al. 2013; Lynch et al. 2016, e.g.). Recently, Richey-Yowell et al. (2020) showed that infrared photometric variability at 0.5–4 μm does not trace quiescent radio emission, but they reaffirm an earlier finding by Pineda et al. (2017) that Hα emission is correlated with the quiescent radio emission of ultracool dwarfs that have detected radio aurorae. Excluding these objects removes any obvious bias for magnetic activity in our samples. With the exception of the Kao et al. (2016) study, other survey attempts to introduce a positive detection bias have not yielded detection rates that are distinct from volume-limited studies (e.g. Richey-Yowell et al. 2020). Similarly, attempts to target individual objects that may be promising have yielded mixed results (e.g. Audard et al. 2005; Pineda & Hallinan 2018). We therefore elect to include all remaining available data to allow the hypothetical effects of these various selection attempts to average out.

For both datasets, we repeat this calculation for four luminosity distribution cases. We summarize these calculations in Table 2. In all cases, binary ultracool dwarfs have an elevated quiescent radio occurrence rate.

5 DISCUSSION

Comparing binary versus single-object systems gives strong evidence that binarity may enhance the occurrence rate of quiescent radio activity in ultracool dwarfs. One possible contributor to the high binary occurrence rate may be that some of the included binary systems are in fact unresolved triples. With higher multiplicity, a greater fraction of combinations of radio-bright individual components can result in an unresolved system appearing radio-bright as a whole. However, ultracool dwarf triple systems are very rare (Bardalez Gagliuffi et al. 2014), and we have excluded all targets that have evidence of higher-order multiplicity. Our results imply that binaries are excellent targets for radio studies that aim to increase the number of known radio-bright ultracool dwarfs because they may have an elevated radio occurrence rate compared to single objects.

The radio occurrence rates that we report are specifically for non-flaring non-thermal radio emission. Since the quiescent emission that we focus on does not directly trace flares, our finding that binarity enhances the ultracool dwarf quiescent radio occurrence rate raises interesting questions about the plasma source for this emission.

Table 2. Calculated occurrence rates

Dataset	Sample Size (binary, single)	$\mathcal{P}(L_{\nu,\mathrm{single}})$ $e = 1$	$L_{\mathrm{min}}, L_{\mathrm{max}}$ $e = 1$	θ_{binary}	$\theta_{\mathrm{predict}}$	$\mathbb{P}(\theta_{\mathrm{binary}} > \theta_{\mathrm{predict}})$
Literature	28, 112	Uniform	11.7–13.6	$0.58^{+0.10}_{-0.11}$	$0.22^{+0.08}_{-0.07}$	100%
Literature	28, 112	Uniform	9.8–13.6	$0.59^{+0.10}_{-0.11}$	$0.23^{+0.08}_{-0.07}$	100%
Literature	28, 112	KM	11.7–13.6	$0.67^{+0.11}_{-0.12}$	$0.27^{+0.09}_{-0.08}$	100%
Literature	28, 112	KM	9.8–13.6	$0.68^{+0.11}_{-0.12}$	$0.28^{+0.09}_{-0.08}$	100%
no K16 [a]	27, 54	Uniform	11.7–13.6	$0.56^{+0.11}_{-0.11}$	$0.16^{+0.12}_{-0.09}$	100%
no K16 [a]	27, 54	Uniform	9.8–13.6	$0.57^{+0.11}_{-0.11}$	$0.16^{+0.12}_{-0.09}$	100%
no K16 [a]	27, 54	KM	11.7–13.6	$0.64^{+0.11}_{-0.12}$	$0.20^{+0.14}_{-0.11}$	100%
no K16 [a]	27, 54	KM	9.8–13.6	$0.65^{+0.11}_{-0.12}$	$0.20^{+0.14}_{-0.11}$	100%

Note – For the single sample, single objects were randomly drawn from a samples of 82 ultracool M dwarfs, 74 L dwarfs, and 23 T/Y dwarfs to match the spectral type distribution of the individual components in the binary sample. Listed values are calculated from the mean distribution of 1000 trials. Reported uncertainties correspond to 68.3% credible intervals.

[a] Excluding observations from Kao et al. (2016, 2018) to reduce possible bias from their selection effects.

A binary enhancement effect suggests that volcanic activity from satellites may not be the dominant source of magnetospheric plasma emission for ultracool dwarfs. Planet occurrence rates are suppressed for close-in binary stellar systems compared to wide-separation binaries and single-star systems (Moe & Kratter 2019). Theory suggests that this suppression occurs because binaries can truncate the mass and radius of the circumprimary disk, increase disk turbulence, and/or clear out disk material on timescales faster than planet formation (e.g., Artymowicz & Lubow 1994; Haghighipour & Raymond 2007; Rafikov & Silsbee 2015). Like stars, ultracool dwarfs are known to host planets (e.g. the TRAPPIST-1 system, Gillon et al. 2017) and theory predicts multiple rocky planets around brown dwarfs (He et al. 2017). Thus, similar mechanisms may suppress planet formation around close-in brown dwarf binaries. In this scenario, we would also expect a suppressed quiescent radio occurrence rate if volcanic satellites are a key electron source. We emphasize, however, that our results do not rule out this mechanism. Instead, our results suggest that some other mechanism may on average outweigh the contribution of volcanic activity from satellites.

We additionally rule out excess flaring induced by magnetic interactions (e.g. Morgan et al. 2012; Lanza 2012). The smallest separation binaries in our sample ($\sim$ 0.6 AU) rule out significant magnetospheric interactions. The strongest ultracool dwarf dipole fields (~5 kG Kao et al. 2018) will decay by $1/r^3$ to $\lesssim$ 20 nG at the half-way point between binary components, which is less than ISM field strengths (Sofue et al. 2019).

One possibility may be that flaring activity provides a significant source of plasma for ultracool dwarf quiescent radio emission. For example, though no flares on T dwarfs have been detected yet, recent studies demonstrate that flares can occur on objects that are at least as late as L5 (Paudel et al. 2018a; Jackman et al. 2019; Paudel et al. 2020). If flaring activity seeds the magnetospheric plasma of ultracool dwarfs, then ultracool dwarf binaries may experience significant rotation-enhanced flaring. As noted in our introduction, tidal spin-up may enhance the rotation rates of stars and thus the magnetic activity of the stellar binary population (Zahn 1977; Morgan et al. 2016). Similar phenomena may occur for ultracool dwarfs. Alternatively, higher binary rotation rotation rates can result from shorter disk dissipation timescales in binary systems (Scholz et al. 2018).

However, existing studies suggest that flare activity may not correlate with radio activity. A study of flare frequency rates spanning M6–L0 spectral types suggests that flare frequencies decrease with later spectral types (Paudel et al. 2018a). Similarly, activity strengths of the chromospheric activity marker Hα decrease with later spectral types (Schmidt et al. 2015; Pineda et al. 2017). If flares indeed correlate with radio emission, we expect the latest type ultracool dwarfs to similarly exhibit a lower radio occurrence rate when all other factors are equal. Intriguingly, a comparison of quiescent radio occurrence rates between M, L and T/Y dwarfs tentatively demonstrates that while L dwarfs may have a lower radio occurrence rate than M dwarfs, T/Y dwarfs may not have a lower rate than L dwarfs (Kao & Shkolnik submitted). These findings tentatively suggest that flaring activity may not significantly contribute to the plasma reservoir that quiescent radio emission traces. While Kao & Shkolnik (submitted) do not control for other possible confounding factors such as age or rotation rate, their findings support evidence that radio ultracool dwarfs exhibit Hα activity that is distinct from flare activity (Pineda et al. 2017; Richey-Yowell et al. 2020).

Gaining further insight into flare contributions to the plasma reservoir traced by ultracool dwarf quiescent radio emission will require studies that (1) examine how rotation rates correlate with ultracool dwarf flare rates and (2) compare the quiescent radio occurrence rate for flaring versus non-flaring ultracool dwarfs. If such studies find a higher occurrence rate of quiescent radio emission in flaring versus non-flaring objects, this may imply that flares provide a significant source of plasma in the magnetospheres of ultracool dwarfs.

6 CONCLUSIONS

We present the first detailed statistical comparison of non-flaring quiescent radio emission in ultracool dwarf binary systems compared to their single-object counterparts. Prior to this work, detection rate studies did not account for possible effects of binarity.

We compile all published radio observations of binary ultracool dwarfs and compare the radio luminosities of binary systems to single objects.

We show that although binarity previously appeared to possibly enhance the quiescent radio luminosities of detected ultracool dwarf binary systems relative to single objects, controlling for spectral types may account for this observed phenomenon.

Finally, we show how to apply a generalized analytical Bayesian framework for calculating the occurrence rate of steady emission in astrophysical populations introduced by Kao & Shkolnik (submitted) to comparisons between binary versus single-object systems in a rigorous and self-consistent manner. We then compare the quiescent radio occurrence rate of ultracool dwarf binary systems to single objects with a similar spectral type distribution as for our binary sample and find that binarity enhances the the quiescent radio occurrence rate in ultracool dwarfs compared to their single counterparts.

ACKNOWLEDGEMENTS

MK specially thanks Cameron Voloshin for valuable statistics and software engineering discussions that shaped this work, Jackie Villadsen for her help in troubleshooting target calibration and imaging, and Adam Schneider for serving as a valuable resource on brown dwarf binaries. She also thanks her Magnetism & Equity group for their support during the Covid-19 pandemic, which Support was provided by NASA through the NASA Hubble Fellowship grant HST-HF2-51411.001-A awarded by the Space Telescope Science Institute, which is operated by the Association of Universities for Research in Astronomy, Inc., for NASA, under contract NAS5-26555; and by the Heising-Simons Foundation through the 51 Pegasi b Fellowship grant 2021-2943. This work is based on observations made with the NSF's Karl G. Jansky Very Large Array (VLA). This research has made use of the SIMBAD and VizieR databases, operated at CDS, Strasbourg, France; and the European Space Agency (ESA) mission *Gaia* (https://www.cosmos.esa.int/gaia), processed by the Gaia Data Processing and Analysis Consortium (DPAC, https://www.cosmos.esa.int/web/gaia/dpac/consortium).

Software: CASA (McMullin et al. 2007), Astropy (Price-Whelan et al. 2018), Matplotlib (Hunter 2007), Numpy (van der Walt et al. 2011), Scipy (Jones et al. 2001), Scikit-learn (Pedregosa et al. 2011).

DATA AVAILABILITY

This work is a meta-analysis of previously published radio observations of ultracool dwarfs. As such, all data used in this study have been compiled in table format in Kao & Shkolnik (submitted) and Kao & Pineda (accepted).

REFERENCES

Antonova, A., Doyle, J. G., Hallinan, G., Golden, A., & Koen, C. 2007, A&A, 472, 257, doi: 10.1051/0004-6361:20077231
Antonova, A., Hallinan, G., Doyle, J. G., et al. 2013, A&A, 549, A131, doi: 10.1051/0004-6361/201118583
Artymowicz, P., & Lubow, S. H. 1994, ApJ, 421, 651, doi: 10.1086/173679
Audard, M., Brown, A., Briggs, K. R., et al. 2005, ApJ, 625, L63, doi: 10.1086/430881
Bardalez Gagliuffi, D. C., Gelino, C. R., & Burgasser, A. J. 2015, AJ, 150, 163, doi: 10.1088/0004-6256/150/5/163
Bardalez Gagliuffi, D. C., Burgasser, A. J., Gelino, C. R., et al. 2014, ApJ, 794, 143, doi: 10.1088/0004-637X/794/2/143
Basharinov, A. E., Gurvich, A. S., & Egorov, S. T. 1974, Moscow Izdatel Nauka
Berger, E. 2002, ApJ, 572, 503, doi: 10.1086/340301
—. 2006, ApJ, 648, 629, doi: 10.1086/505787
Berger, E., Ball, S., Becker, K. M., et al. 2001, Nature, 410, 338
Berger, E., Rutledge, R. E., Reid, I. N., et al. 2005, ApJ, 627, 960, doi: 10.1086/430343
Blunt, S., Nielsen, E. L., De Rosa, R. J., et al. 2017, AJ, 153, 229, doi: 10.3847/1538-3881/aa6930
Bolton, S. J., Thorne, R. M., Bourdarie, S., de Pater, I., & Mauk, B. 2004, Jupiter's inner radiation belts, ed. F. Bagenal, T. E. Dowling, & W. B. McKinnon, 671–688
Bouy, H., Brandner, W., Martín, E. L., et al. 2003, AJ, 126, 1526, doi: 10.1086/377343
Bouy, H., Martín, E. L., Brandner, W., & Bouvier, J. 2005, AJ, 129, 511, doi: 10.1086/426559
Bouy, H., Duchêne, G., Köhler, R., et al. 2004, A&A, 423, 341, doi: 10.1051/0004-6361:20040551
Burgasser, A. J., Cruz, K. L., Cushing, M., et al. 2010, ApJ, 710, 1142, doi: 10.1088/0004-637X/710/2/1142
Burgasser, A. J., Kirkpatrick, J. D., & Lowrance, P. J. 2005, AJ, 129, 2849, doi: 10.1086/430218
Burgasser, A. J., & McElwain, M. W. 2006, AJ, 131, 1007, doi: 10.1086/499042
Burgasser, A. J., Melis, C., Todd, J., et al. 2015a, AJ, 150, 180, doi: 10.1088/0004-6256/150/6/180
Burgasser, A. J., Melis, C., Zauderer, B. A., & Berger, E. 2013a, ApJ, 762, L3, doi: 10.1088/2041-8205/762/1/L3
Burgasser, A. J., Sheppard, S. S., & Luhman, K. L. 2013b, ApJ, 772, 129, doi: 10.1088/0004-637X/772/2/129
Burgasser, A. J., Sitarski, B. N., Gelino, C. R., Logsdon, S. E., & Perrin, M. D. 2011a, ApJ, 739, 49, doi: 10.1088/0004-637X/739/1/49
Burgasser, A. J., Cushing, M. C., Kirkpatrick, J. D., et al. 2011b, ApJ, 735, 116, doi: 10.1088/0004-637X/735/2/116
Burgasser, A. J., Gillon, M., Melis, C., et al. 2015b, AJ, 149, 104, doi: 10.1088/0004-6256/149/3/104
Clarke, J. T., Grodent, D., Cowley, S. W. H., et al. 2004, Jupiter's aurora, ed. F. Bagenal, T. E. Dowling, & W. B. McKinnon, 639–670
Deshpande, R., Martín, E. L., Montgomery, M. M., et al. 2012, AJ, 144, 99, doi: 10.1088/0004-6256/144/4/99
Dieterich, S. B., Henry, T. J., Jao, W.-C., et al. 2014, AJ, 147, 94, doi: 10.1088/0004-6256/147/5/94
Dieterich, S. B., Weinberger, A. J., Boss, A. P., et al. 2018, ApJ, 865, 28, doi: 10.3847/1538-4357/aadadc
Dupuy, T. J., & Liu, M. C. 2012, ApJS, 201, 19, doi: 10.1088/0067-0049/201/2/19

—. 2017, ApJS, 231, 15, doi: 10.3847/1538-4365/aa5e4c
Dupuy, T. J., Liu, M. C., & Ireland, M. J. 2009, ApJ, 692, 729, doi: 10.1088/0004-637X/692/1/729
Dupuy, T. J., Liu, M. C., Best, W. M. J., et al. 2019, AJ, 158, 174, doi: 10.3847/1538-3881/ab3cd1
Faherty, J. K., Burgasser, A. J., Cruz, K. L., et al. 2009, AJ, 137, 1, doi: 10.1088/0004-6256/137/1/1
Faherty, J. K., Burgasser, A. J., Walter, F. M., et al. 2012, ApJ, 752, 56, doi: 10.1088/0004-637X/752/1/56
Forbrich, J., Dupuy, T. J., Reid, M. J., et al. 2016, ApJ, 827, 22, doi: 10.3847/0004-637X/827/1/22
Forrest, W. J., Skrutskie, M. F., & Shure, M. 1988, ApJ, 330, L119, doi: 10.1086/185218
Gaia Collaboration. 2018, VizieR Online Data Catalog, I/345
Ganushkina, N. Y., Dandouras, I., Shprits, Y. Y., & Cao, J. 2011, Journal of Geophysical Research (Space Physics), 116, A09234, doi: 10.1029/2010JA016376
Gauza, B., Béjar, V. J. S., Pérez-Garrido, A., et al. 2015, ApJ, 804, 96, doi: 10.1088/0004-637X/804/2/96
Gelino, C. R., Smart, R. L., Marocco, F., et al. 2014, AJ, 148, 6, doi: 10.1088/0004-6256/148/1/6
Gillon, M., Triaud, A. H. M. J., Demory, B.-O., et al. 2017, Nature, 542, 456, doi: 10.1038/nature21360
Girard, J. N., Zarka, P., Tasse, C., et al. 2016, A&A, 587, A3, doi: 10.1051/0004-6361/201527518
Gizis, J. E. 2002, ApJ, 575, 484, doi: 10.1086/341259
Gizis, J. E., Burgasser, A. J., Berger, E., et al. 2013, ApJ, 779, 172, doi: 10.1088/0004-637X/779/2/172
Golimowski, D. A., Henry, T. J., Krist, J. E., et al. 2004, AJ, 128, 1733, doi: 10.1086/423911
Guenther, E. W., & Wuchterl, G. 2003, A&A, 401, 677, doi: 10.1051/0004-6361:20030149
Guirado, J. C., Azulay, R., Gauza, B., et al. 2018, A&A, 610, A23, doi: 10.1051/0004-6361/201732130
Haghighipour, N., & Raymond, S. N. 2007, ApJ, 666, 436, doi: 10.1086/520501
Hallinan, G., Antonova, A., Doyle, J. G., et al. 2006, ApJ, 653, 690, doi: 10.1086/508678
—. 2008, ApJ, 684, 644, doi: 10.1086/590360
Hallinan, G., Bourke, S., Lane, C., et al. 2007, ApJ, 663, L25, doi: 10.1086/519790
Hallinan, G., Littlefair, S. P., Cotter, G., et al. 2015, Nature, 523, 568, doi: 10.1038/nature14619
He, M. Y., Triaud, A. H. M. J., & Gillon, M. 2017, MNRAS, 464, 2687, doi: 10.1093/mnras/stw2391
Horne, R. B., Thorne, R. M., Glauert, S. A., et al. 2008, Nature Physics, 4, 301 EP . http://dx.doi.org/10.1038/nphys897
Hughes, A. G., Boley, A. C., Osten, R. A., White, J. A., & Leacock, M. 2021, AJ, 162, 43, doi: 10.3847/1538-3881/ac02c3
Hunter, J. D. 2007, Computing in Science and Engineering, 9, 90, doi: 10.1109/MCSE.2007.55
Jackman, J. A. G., Wheatley, P. J., Bayliss, D., et al. 2019, MNRAS, 485, L136, doi: 10.1093/mnrasl/slz039
Jones, E., Oliphant, T., Peterson, P., et al. 2001, SciPy: Open source scientific tools for Python. http://www.scipy.org/
Kao, M. M., Hallinan, G., & Pineda, J. S. 2019, MNRAS, 487, 1994, doi: 10.1093/mnras/stz1372
Kao, M. M., Hallinan, G., Pineda, J. S., et al. 2016, ApJ, 818, 24, doi: 10.3847/0004-637X/818/1/24
Kao, M. M., Hallinan, G., Pineda, J. S., Stevenson, D., & Burgasser, A. 2018, ApJS, 237, 25, doi: 10.3847/1538-4365/aac2d5
Kao, M. M., & Pineda, J. S. accepted, ApJ
Kao, M. M., & Shkolnik , E. submitted, MNRAS
Kaplan, E. L., & Meier, P. 1958, Journal of the American Statistical Association, 53, 457
Kellermann, K. I. 1970, Radio Science, 5, 487, doi: 10.1029/RS005i002p00487
Khurana, K. K., Kivelson, M. G., Vasyliunas, V. M., et al. 2004, The configuration of Jupiter's magnetosphere, ed. F. Bagenal, T. E. Dowling, & W. B. McKinnon, 593–616
Kirkpatrick, J. D., Reid, I. N., Liebert, J., et al. 2000, AJ, 120, 447, doi: 10.1086/301427
Koen, C. 2013, MNRAS, 428, 2824, doi: 10.1093/mnras/sts208
Köhler, R., Ratzka, T., & Leinert, C. 2012, A&A, 541, A29, doi: 10.1051/0004-6361/201118707
Konopacky, Q. M., Ghez, A. M., Barman, T. S., et al. 2010, ApJ, 711, 1087, doi: 10.1088/0004-637X/711/2/1087
Krishnamurthi, A., Leto, G., & Linsky, J. L. 1999, AJ, 118, 1369, doi: 10.1086/301015
Lanza, A. F. 2012, A&A, 544, A23, doi: 10.1051/0004-6361/201219002
Lazorenko, P. F., & Sahlmann, J. 2018, A&A, 618, A111, doi: 10.1051/0004-6361/201833626
Lee, E. T., & Wang, J. W. 2003, Statistical methods for survival data analysis, 3rd edn., Wiley series in probability and statistics (New York: J. Wiley)
Leinert, C., Allard, F., Richichi, A., & Hauschildt, P. H. 2000, A&A, 353, 691
Liu, M. C., Dupuy, T. J., & Allers, K. N. 2016, ApJ, 833, 96, doi: 10.3847/1538-4357/833/1/96
Luhman, K. L. 2013, ApJ, 767, L1, doi: 10.1088/2041-8205/767/1/L1
Lynch, C., Murphy, T., Ravi, V., et al. 2016, MNRAS, 457, 1224, doi: 10.1093/mnras/stw050
Mauk, B. H., & Fox, N. J. 2010, Journal of Geophysical Research (Space Physics), 115, A12220, doi: 10.1029/2010JA015660
McCaughrean, M. J., Scholz, R. D., & Lodieu, N. 2002, A&A, 390, L27, doi: 10.1051/0004-6361:20020928
McElwain, M. W., & Burgasser, A. J. 2006, AJ, 132, 2074, doi: 10.1086/508199
McLean, M., Berger, E., Irwin, J., Forbrich, J., & Reiners, A. 2011, ApJ, 741, 27, doi: 10.1088/0004-637X/741/1/27
McLean, M., Berger, E., & Reiners, A. 2012, ApJ, 746, 23, doi: 10.1088/0004-637X/746/1/23
McMullin, J. P., Waters, B., Schiebel, D., Young, W., & Golap, K. 2007, Astronomical Society of the Pacific Conference Series, Vol. 376, CASA Architecture and Applications, ed. R. A. Shaw, F. Hill, & D. J. Bell, 127
Moe, M., & Kratter, K. M. 2019, arXiv e-prints, arXiv:1912.01699. https://arxiv.org/abs/1912.01699
Morgan, D. P., West, A. A., & Becker, A. C. 2016, AJ, 151, 114, doi: 10.3847/0004-6256/151/5/114
Morgan, D. P., West, A. A., Garcés, A., et al. 2012, AJ, 144, 93, doi: 10.1088/0004-6256/144/4/93
Osten, R. A., Hawley, S. L., Bastian, T. S., & Reid, I. N. 2006, ApJ, 637, 518, doi: 10.1086/498345
Osten, R. A., & Jayawardhana, R. 2006, ApJ, 644, L67, doi: 10.1086/505328
Osten, R. A., Melis, C., Stelzer, B., et al. 2015, ApJ, 805, L3, doi: 10.1088/2041-8205/805/1/L3
Paudel, R. R., Gizis, J. E., Mullan, D. J., et al. 2018a, ApJ, 858, 55, doi: 10.3847/1538-4357/aab8fe
—. 2018b, ApJ, 861, 76, doi: 10.3847/1538-4357/aac8e0
—. 2020, arXiv e-prints, arXiv:2004.10579. https://arxiv.org/abs/2004.10579
Pedregosa, F., Varoquaux, G., Gramfort, A., et al. 2011, Journal of Machine Learning Research, 12, 2825
Pineda, J. S., & Hallinan, G. 2018, ApJ, 866, 155, doi: 10.3847/1538-4357/aae078

Pineda, J. S., Hallinan, G., & Kao, M. M. 2017, ApJ, 846, 75, doi: 10.3847/1538-4357/aa8596
Potter, D., Martín, E. L., Cushing, M. C., et al. 2002, ApJ, 567, L133, doi: 10.1086/339999
Price-Whelan, A. M., Sipócz, B. M., Günther, H. M., et al. 2018, AJ, 156, 123, doi: 10.3847/1538-3881/aabc4f
Rafikov, R. R., & Silsbee, K. 2015, ApJ, 798, 69, doi: 10.1088/0004-637X/798/2/69
Reid, I. N., Cruz, K. L., Kirkpatrick, J. D., et al. 2008, AJ, 136, 1290, doi: 10.1088/0004-6256/136/3/1290
Reid, I. N., Kirkpatrick, J. D., Liebert, J., et al. 2002, AJ, 124, 519, doi: 10.1086/340805
Richey-Yowell, T., Kao, M. M., Pineda, J. S., Shkolnik, E. L., & Hallinan, G. 2020, ApJ, 903, 74, doi: 10.3847/1538-4357/abb826
Route, M., & Wolszczan, A. 2012, ApJ, 747, L22, doi: 10.1088/2041-8205/747/2/L22
—. 2016a, ApJ, 821, L21, doi: 10.3847/2041-8205/821/2/L21
—. 2016b, ApJ, 830, 85, doi: 10.3847/0004-637X/830/2/85
Sault, R. J., Oosterloo, T., Dulk, G. A., & Leblanc, Y. 1997, A&A, 324, 1190
Schmidt, S. J., Cruz, K. L., Bongiorno, B. J., Liebert, J., & Reid, I. N. 2007, AJ, 133, 2258, doi: 10.1086/512158
Schmidt, S. J., Hawley, S. L., West, A. A., et al. 2015, AJ, 149, 158, doi: 10.1088/0004-6256/149/5/158
Scholz, A., Moore, K., Jayawardhana, R., et al. 2018, ApJ, 859, 153, doi: 10.3847/1538-4357/aabfbe
Scholz, R. D., McCaughrean, M. J., Lodieu, N., & Kuhlbrodt, B. 2003, A&A, 398, L29, doi: 10.1051/0004-6361:20021847
Sestovic, M., & Demory, B.-O. 2020, A&A, 641, A170, doi: 10.1051/0004-6361/202037732
Siegler, N., Close, L. M., Cruz, K. L., Martín, E. L., & Reid, I. N. 2005, ApJ, 621, 1023, doi: 10.1086/427743
Smart, R. L., Tinney, C. G., Bucciarelli, B., et al. 2013, MNRAS, 433, 2054, doi: 10.1093/mnras/stt876
Sofue, Y., Nakanishi, H., & Ichiki, K. 2019, MNRAS, 485, 924, doi: 10.1093/mnras/stz407
Stone, J. M., Skemer, A. J., Kratter, K. M., et al. 2016, ApJ, 818, L12, doi: 10.3847/2041-8205/818/1/L12
Stumpf, M. B., Brandner, W., Bouy, H., Henning, T., & Hippler, S. 2010, A&A, 516, A37, doi: 10.1051/0004-6361/200913711
Tinney, C. G., Faherty, J. K., Kirkpatrick, J. D., et al. 2014, ApJ, 796, 39, doi: 10.1088/0004-637X/796/1/39
van der Walt, S., Colbert, S. C., & Varoquaux, G. 2011, Computing in Science and Engineering, 13, 22, doi: 10.1109/MCSE.2011.37
Vedantham, H. K., Callingham, J. R., Shimwell, T. W., et al. 2020, ApJ, 903, L33, doi: 10.3847/2041-8213/abc256
Villadsen, J., & Hallinan, G. 2019, ApJ, 871, 214, doi: 10.3847/1538-4357/aaf88e
Villadsen, J., Hallinan, G., Bourke, S., Güdel, M., & Rupen, M. 2014, ApJ, 788, 112, doi: 10.1088/0004-637X/788/2/112
Weinberger, A. J., Boss, A. P., Keiser, S. A., et al. 2016, AJ, 152, 24, doi: 10.3847/0004-6256/152/1/24
Williams, P. K. G., & Berger, E. 2015, ApJ, 808, 189, doi: 10.1088/0004-637X/808/2/189
Williams, P. K. G., Berger, E., Irwin, J., Berta-Thompson, Z. K., & Charbonneau, D. 2015a, ApJ, 799, 192, doi: 10.1088/0004-637X/799/2/192
Williams, P. K. G., Casewell, S. L., Stark, C. R., et al. 2015b, ApJ, 815, 64, doi: 10.1088/0004-637X/815/1/64
Williams, P. K. G., Cook, B. A., & Berger, E. 2014, ApJ, 785, 9, doi: 10.1088/0004-637X/785/1/9
Williams, P. K. G., Gizis, J. E., & Berger, E. 2017, ApJ, 834, 117, doi: 10.3847/1538-4357/834/2/117
Zahn, J. P. 1977, A&A, 500, 121
Zhang, Q., Hallinan, G., Brisken, W., Bourke, S., & Golden, A. 2020, ApJ, 897, 11, doi: 10.3847/1538-4357/ab9177

This paper has been typeset from a TEX/LATEX file prepared by the author.